

Large-area regular nanodomain patterning in He-irradiated lithium niobate crystals

This article has been downloaded from IOPscience. Please scroll down to see the full text article.

2011 Nanotechnology 22 285309

(<http://iopscience.iop.org/0957-4484/22/28/285309>)

View [the table of contents for this issue](#), or go to the [journal homepage](#) for more

Download details:

IP Address: 130.209.6.41

The article was downloaded on 05/04/2012 at 15:50

Please note that [terms and conditions apply](#).

Large-area regular nanodomain patterning in He-irradiated lithium niobate crystals

A Ofan¹, M Lilienblum², O Gaathon¹, A Sehrbrock³,
Á Hoffmann², S Bakhru⁴, H Bakhru⁴, S Irsen³, R M Osgood Jr¹
and E Soergel²

¹ Center for Integrated Science and Technology, Columbia University, New York, NY 10027, USA

² Institute of Physics, University of Bonn, Wegelerstraße 8, 53115 Bonn, Germany

³ Center of Advanced European Studies and Research (CAESAR), Ludwig-Erhard-Allee 2, 53175 Bonn, Germany

⁴ College of Nanoscale Science and Engineering, State University of New York at Albany, Albany, NY 12222, USA

E-mail: ao2199@columbia.edu and soergel@uni-bonn.de

Received 24 December 2010, in final form 2 May 2011

Published 7 June 2011

Online at stacks.iop.org/Nano/22/285309

Abstract

Large-area ferroelectric nanodomain patterns, which are desirable for nonlinear optical applications, were generated in previously He-implanted lithium niobate crystals by applying voltage pulses to the tip of a scanning force microscope. The individual nanodomains were found to be of uniform size, which depended only on the inter-domain spacing and the pulse amplitude. We explain this behavior by the electrostatic repulsion of poling-induced buried charges between adjacent domains. The domain patterns were imaged by piezoresponse force microscopy and investigated by domain-selective etching in conjunction with focused ion beam etching followed by scanning electron microscopy imaging.

In order to optimize the He-irradiation parameters for easy and reliable nanodomain patterning a series of samples subjected to various irradiation fluences and energies was prepared. The different samples were characterized by investigating nanodomains generated with a wide range of pulse parameters (amplitude and duration). In addition, these experiments clarified the physical mechanism behind the facile poling measured in He-irradiated lithium niobate crystals: the damage caused by the energy loss that takes place via electronic excitations appears to act to stabilize the domains, whereas the nuclear-collision damage degrades the crystal quality, and thus impedes reliable nanodomain generation.

1. Introduction

Ferroelectric lithium niobate (LiNbO₃) has outstanding acousto-optic, nonlinear optical, electro-optic, and photorefractive properties [1, 2]. Various applications ranging from photorefractive data storage [3] to advanced photonic applications [4] have been reported. The most prominent example is efficient frequency conversion using quasi-phase matching (QPM) in periodically poled crystals [5]. The range of accessible wavelengths using QPM for frequency-doubling, however, is limited by the minimum size of the

available periodicity of the domain patterns: to date periods in the few-to-sub-micrometer regime are not readily obtainable. Indeed such domain patterns are also needed for back-wave QPM [6, 7].

Recently, photonic crystals have gained increased attention as they allow controlling the light propagation for specific applications via the periodic alteration of the dielectric constant [8]. Due to its excellent optical properties, LiNbO₃ is an important platform material for integrated optical applications [9], and the implementation of a photonic crystal structure in LiNbO₃ is therefore of much interest [10].

However, topographical structuring of a crystal surface for photonic crystal applications usable at visible wavelengths is still challenging. This application requires a large-area regular pattern whereby the individual structures are sized in the sub-micron range. Several techniques, such as ion beam enhanced etching (IBEE) [11], focused ion beam (FIB) milling [12, 13], laser ablation [14], and plasma-etching [15], have been used to attempt fabricating such patterns. A different approach for topographical structuring of LiNbO₃ crystals utilizes domain-selective etching [16]. This technique has been proven to be very versatile, and recently ridge waveguides [17], and whispering gallery mode resonators [18] have been fabricated. The utilization of this technique for the fabrication of photonic crystals requires sub-micrometer-sized individual domains regularly arranged in a large-area pattern.

The standard technique for domain inversion is electric-field poling (EFP) using structured electrodes to locally apply an electric field exceeding the coercive field E_c required for domain inversion. This technique, however, fails when small, sub-micrometer-sized domains are required. The central difficulty in fabricating such domain patterns is that in standard EFP unwanted sideways growth of the domains occurs due to the unfavorable electric-field distribution inside the crystal, thus greatly limiting the minimum domain size. For the same reason neighboring domains tend to merge during EFP. Attempts to improve domain formation by ultraviolet (UV)-light assistance [19, 20] or elevated temperatures [21] have not, to date, reached the desired results in sub-micrometer domain formation.

Recently it has been shown that sub-micrometer-sized surface domains can be written in He-irradiated LiNbO₃ crystals by applying voltage pulses to the tip of a scanning probe microscope [22]. In this paper, we present a detailed analysis of this technique and in particular the dependence of the domain formation on both the pulse (voltage and duration) and the irradiation parameters (energy and fluence), hence providing a deeper understanding of the poling process. In view of the applicability of domains generated in this way, we present data on their shape and demonstrate the fabrication of a large-area regular domain pattern, which has the potential to be used for photonic nano- or micro-components.

2. Experimental methods

In our experiment 500 μm -thick congruent LiNbO₃ wafers, including those doped with 5% Mg, were used. The wafers were cut to the desired sample size and irradiated with He⁺ ions through their +z face (figure 1(a)) with fluences between 1×10^{14} and $5 \times 10^{16} \text{ cm}^{-2}$ at energies ranging from 130 keV to 3.8 MeV, corresponding to an implantation depth of 0.5–10 μm , respectively. A more detailed description of the sample preparation can be found in [23]. The inclusion of Mg-doped crystals into our investigations is basically for two reasons: (i) 5% Mg-doped LiNbO₃ is the material of choice for nonlinear optical applications, as it does not show photorefractive optical damage [24]; and (ii) the coercive field E_c is smaller by one order of magnitude when compared to undoped LiNbO₃ [25], and can even be reduced further by

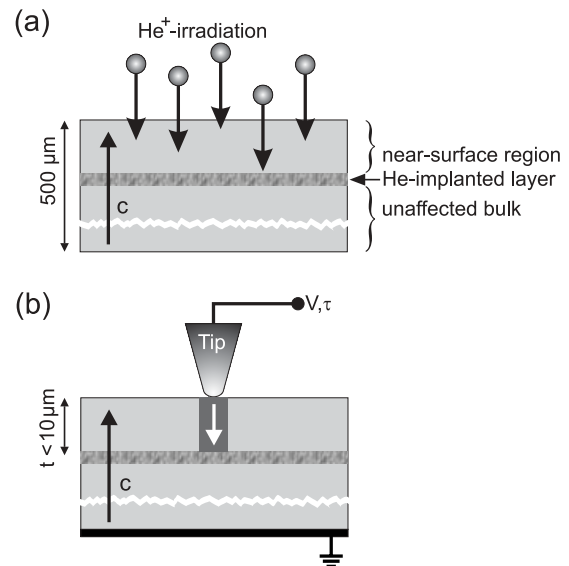


Figure 1. (a) Schematic illustration of the He-irradiated LiNbO₃ samples and notations used in the text for the different areas of the samples. (b) A sketch showing the principle of local domain formation with a scanning probe microscope tip by application of voltage pulses of amplitude V and duration τ . The implantation depth is denoted by t .

UV illumination [26]. In addition it has been observed that the electrical conductivity of Mg-doped LiNbO₃ is increased strongly by UV illumination [27].

The poling performance of the He-irradiated samples was investigated by ‘poling maps’ where scanning probe microscopy (SPM) was used for generation and subsequent analysis of domain patterns (section 2.1). The modification of selected physical properties of the irradiated region was studied using piezoresponse force microscopy (PFM) and electrostatic force microscopy (EFM) by investigating cross-sections of the samples (section 2.2). The shape of the domains was examined using FIB milling and scanning electron microscopy (SEM) imaging of selective etched domains (section 2.3). The experimental details for carrying out these measurements are laid out in the following sections.

2.1. Poling maps

To study the poling performance of the He-irradiated samples domain patterns were formed by locally applying voltage pulses to the tip of an SPM (Solaris NT-MDT) as shown schematically in figure 1(b). The use of a custom-designed scripting program allowed automation of the domain formation of a grid of domains (termed a poling map) using varying poling voltages V and pulse durations τ , for a range of V from -100 to $+100$ V and τ from 1 ms to 100 s. In addition, large-area domain patterns, up to $100 \times 100 \mu\text{m}^2$, were generated using this scripting, whereby the individual domains were written with identical voltage pulses. Here the inter-domain spacing was varied between of 0.5 and 8 μm . All domain patterns were studied by PFM through applying an alternating voltage $V_{ac} = 5 V_{rms}$ of frequency ≈ 30 kHz to the SPM tip. The tips utilized for writing and imaging were diamond coated

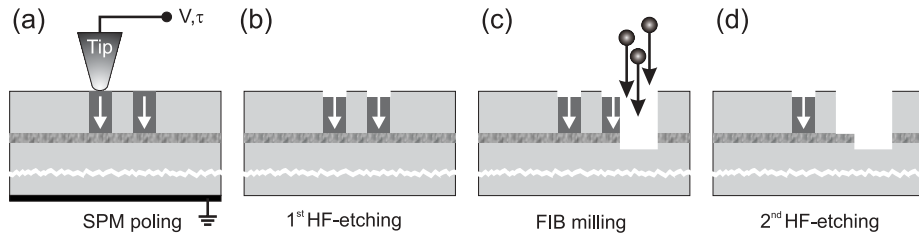


Figure 2. Schematic illustration of the process used to investigate the domain shape. First domains are formed in an He-irradiated LiNbO₃ using a SPM tip (a), then the location of the domains is determined by a brief selective etch in 48% HF (b). FIB milling is used to open a gap with one boundary lying across the domains (c), followed by a second selective etching in HF that reveals the domains shape (d).

with a nominal radius of $r = 50\text{--}70$ nm (DCP11, NT-MDT). The lateral resolution of PFM images in bulk samples using such tips is limited to ≈ 75 nm [28] and the maximum visible depth to ≈ 1.5 μm [29]. Although the use of sharper tips, and thus better lateral resolution, would have been desirable, the need for using a highly mechanically resistant coating to ensure reproducible long-term domain generation limited the tip choice.

2.2. Investigation of cross-section samples by SPM

To qualify the modifications of the crystal's irradiated areas, we investigated their piezoelectric and electric characteristics. Thus cross-section samples were fabricated by first cutting the crystal into two pieces using a diamond saw and then bonding the two surfaces together using an epoxy-phenolic resin (M-Bond 610). The cross-section was then optically polished to allow for SPM investigations. The piezoresponse, conductivity and permittivity of the near-surface region, the implanted layer and the unaffected bulk were investigated using PFM [30] and electrostatic force microscopy (EFM) [31]. PFM and EFM measurements were performed with the same SPM setup, where for PFM contact mode and for EFM the non-contact mode operation was utilized [32]. The face of the cross-sections to be investigated was either an x or a y -face. For the EFM measurements, the fact that a non-polar face was investigated is of major importance, since EFM investigations on the z -face are, if at all possible, not conclusive due to the large built-in surface polarization charging of LiNbO₃ [33]. The samples were mounted with their z axis perpendicular to the cantilever in order to obtain a maximum amplitude of the lateral PFM signal [34]. To map the fixed charge carrier density the EFM signal at the frequency of the oscillating voltage applied to the tip was read out. To gain information on the local conductivity, i.e. the free charge carrier distribution, and the permittivity of the sample we recorded the EFM signal at twice the frequency of the oscillating voltage applied to the tip [32].

2.3. Domain shape

PFM gives an excellent image of the domain patterns at the surface, however, it does not allow for detailed depth information. We therefore used domain-selective etching in hydrofluoric acid (HF) in conjunction with subsequent SEM imaging to reveal the shape of the domains. The etch rates for

LiNbO₃ in 48% HF are 10 nm min^{-1} for the $-z$ face compared to less than 1 nm h^{-1} for the $+z$ face [35]. In addition, the y -faces are also etched selectively in HF, the $-y$ face at a rate of 90 nm h^{-1} and the $+y$ face at 45 nm h^{-1} [36]. As a consequence, long-term etching of a domain pattern results in a topology, which does not reflect the domain's shape accurately due to lateral etching. In order to minimize this lateral-etching effect only a brief 10 min etch of the crystal was used to mark the domains. A FIB was then employed to open a gap with one boundary lying across the domains and perpendicular to a $-y$ face. By repeated HF etching (again for 10 min), now directly attacking the $-y$ face, the domain's shape could be revealed and subsequently imaged by SEM. For clarification, see the schematic illustration of the process in figure 2.

3. Results

3.1. Poling maps

Poling maps, such as the one shown in figure 3, are used for comparing the poling characteristics of samples irradiated at different conditions. In this example, the crystal was irradiated with a fluence of $10^{14}\text{ He}^+\text{ cm}^{-2}$ at an energy of 130 keV and thus an implantation depth of $t = 0.5\text{ }\mu\text{m}$. Domains at an inter-domain spacing of $3\text{ }\mu\text{m}$ were formed by voltage pulses applied to the SPM tip using different pulse parameters: the amplitude V was chosen between 10 and 100 V, and the duration τ between 1 ms and 100 s. Obviously the size of the domains generated depends on the parameters of the pulse used. More precisely two basic features can be indicated. The size of the formed domain increases linearly with increasing pulse amplitude, but is independent of the pulse duration. This behavior on V and on τ was found to be valid for all samples investigated. From the poling map in figure 3(a) an increase of the domain diameter D with increasing voltage of 3.5 nm V^{-1} can be deduced. The left column shows the smallest domains obtained with $D = 35\text{ nm}$. Note the domain size was confirmed by scanning the area with a sharper tip.

Poling maps were also used to obtain a comparative picture of the domain size as a function of inter-domain spacing. Figures 3(b) and (c) show PFM images of two large-area patterns, with different inter-domain spacings ($1\text{ }\mu\text{m}$ (b) and $0.5\text{ }\mu\text{m}$ (c)), each individual domain generated by an identical voltage pulse of $V = +100\text{ V}$ and $\tau = 1\text{ s}$. The domains were written line by line, starting from the bottom left of the pattern, with the vertical axis as the slow axis. Both

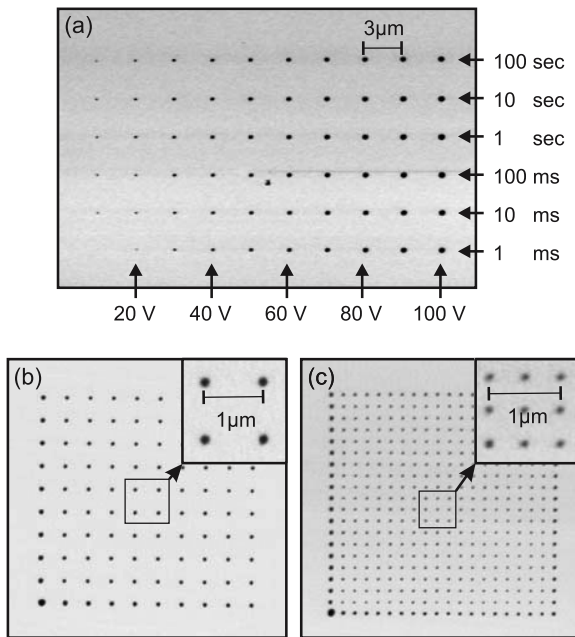


Figure 3. Poling maps obtained for LiNbO₃ irradiated with 10^{14} He⁺ cm⁻² at 130 keV. (a) Varying the pulse parameters as indicated at the sides of the PFM image. The inter-domain spacing is 3 μm, the image size is 33×22 μm². (b) and (c) All individual domains written with voltage pulses of +100 V for 1 s. The inter-domain distance in the patterns is 1 μm (b) and 0.5 μm (c).

patterns show the formation of a ‘frame’, i.e. the domains along the border of the square are larger with respect to those in the center. This effect is more prominent in figure 3(c), where the distance between adjacent domains is smaller. In addition, for both patterns the domain written first (at the bottom left of each pattern) is the largest. Finally, it is observed that the size of the individual central domains is different within the two patterns, 230 and 140 nm diameter for the inter-domain spacings of 1 and 0.5 μm, respectively. In the following we will term the effect of the domains on each other, as described above, by the term ‘proximity effect’.

Finally, poling maps were also written in 5% Mg:LiNbO₃ crystals, on the one hand to determine the applicability of our technique for domain formation in this important material, and on the other hand to take advantage of its lower coercive field E_c for possibly easier domain formation. In addition, the samples were potentially illuminated during domain patterning with a UV lamp (Linus LQ 1000; spectral range: 250–450 nm),

therefore increasing the electrical conductivity of the material even further. However, the results obtained for 5% Mg:LiNbO₃ showed no change with respect to the undoped LiNbO₃, neither for the domain growth nor for the proximity effect, irrespective of an additional UV illumination.

3.2. Investigation of cross-section samples by SPM

The effect of He implantation on the piezoelectricity of the sample was examined by PFM measurements of cross-section samples. For samples irradiated with high fluence and high energy (5×10^{16} cm⁻² at 3.8 MeV), the piezoresponse of the implanted layer was degraded to only $\approx 15\%$ from that of the unaffected bulk, while the near-surface region was reduced by only $\approx 10\%$ [22]. Thus, the implanted layer was basically no longer piezoelectric, whereas the near-surface region was only marginally affected by the He-irradiation. For samples subjected to small fluence ($\leq 1 \times 10^{15}$ cm⁻²), the implanted layer showed no reduction in piezoresponse, irrespective of the energy used for the He-irradiation.

Using EFM we measured the dielectric constant, conductivity, and additional free charge carriers generated by UV illumination, the latter in particular for the Mg-doped samples. Interestingly, none of these parameters were found to be affected by He-irradiation for any of the samples investigated. From the EFM signal we could clearly distinguish between the crystal area and the bonding stripe. This result ascertains that EFM is operating correctly. As for the negative result on the influence of He implantation on the dielectric constant and free charge carrier density, we can only state that either the measurement is not sensitive enough to see the changes or there are no changes to be seen.

3.3. Domain shape

Figure 4(a) shows an SEM image of a domain-patterned crystal after a 10 min HF etching. The individual domains were written by applying 1 s pulses of +100 V on the +z face of a LiNbO₃ crystal He-irradiated with 10^{14} He⁺ cm⁻² at 350 keV, corresponding to an implantation depth of $t = 1$ μm. The etchant attacks only on the -z face, thus the written domains appear as holes in the topography. The result of FIB milling to open a gap followed by a second selective HF etching to reveal the shape of the domains is best seen in figure 4(b). Here also the effect of substantial lateral etching of the holes can be observed: the holes become (i) generally larger, and (ii) evolve toward a distorted hexagonal shaped form (figure 4(c)). The

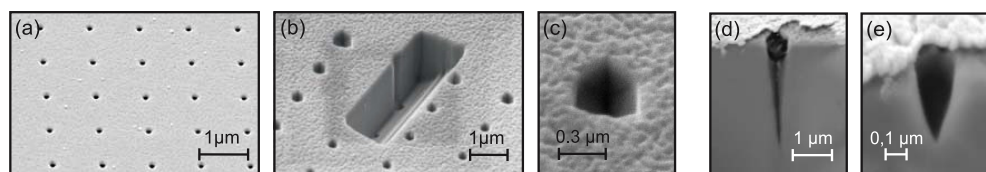


Figure 4. SEM images of etched domain patterns in LiNbO₃ crystals He-irradiated with 10^{14} He⁺ cm⁻² at 350 keV (a)–(c) and 1 MeV (d) and (e). The domains were formed by voltage pulses of $V = +100$ V and $\tau = 1$ s. The topography after a 10 min etch is shown in (a). For (b)–(e) the samples underwent the multi-step procedure described in section 2.3. The hexagonal shape owing to long-term etching is best seen in the zoom image in (c). The closest neighboring domain distance is 4 μm (d) and 0.5 μm (e). The denser pattern results in smaller and shallower domains.

latter reflects the six-fold symmetry of the crystal and the different etch rates for the $+y$ - and the $-y$ -faces.

Figures 4(d) and (e) show SEM images of a crystal after the multi-step procedure to reveal the domain shape. The domains were written by applying 1 s pulses of +100 V on the $+z$ face of a LiNbO₃ crystal He-irradiated with 10^{14} He⁺ cm⁻² at 1 MeV corresponding to an implantation depth of $t = 2.28$ μ m. For the sample with the larger inter-domain spacing (4 μ m), the domain reached the He layer (figure 4(d)). However in the case of the 0.5 μ m inter-domain spacing, a domain of only less than 0.5 μ m depth formed (figure 4(e)). The diameter of the domains at the sample surface, as seen in figures 3(b) and (c), was found to depend on the inter-domain spacing, i.e. 500 nm for the broadly spaced pattern and 200 nm for the narrower pattern. The shape of both these domains is seen to be conical.

The results described above can be summarized as follows: (i) the maximum domain depth corresponds to the depth of the implanted layer and (ii) the proximity effect reduces domain diameter and depth.

4. Discussion

Achieving a better understanding of the physical reasons behind the ease of poling of sub-micrometer-sized domains in He-implanted material was the main goal of our investigations. We will therefore first briefly review the physics of ion irradiation damage in solids (section 4.1) and in light of this background analyze our results on the poling behavior observed in the variation of poling parameters when making poling maps (section 4.2).

The proximity effect, the self-regulation of the size of individual domains within a large-area domain pattern, is one of the most important findings of this study as it is this feature that paves the way for this domain formation technique to reach true applicability. Thus, in section 4.3 we discuss in detail the proximity effect and propose a possible physical explanation. Finally, the shape of the domains is of major importance for practical issues, particularly for the transfer of the domain patterns into a topographical structure. We will discuss these issues in section 4.4.

4.1. Ion irradiation damage in solids

In order to provide background on the ion-implantation physics, a short review of the known lattice effect [37] during irradiation is provided. Specifically, energetic ions penetrating the crystal lattice lose their energy via two dominant binary-collision mechanisms, namely inelastic collisions leading to electronic excitation and elastic collisions leading to crystal damage. Electronic collisions involve only excitation of the lattice electrons, resulting in negligible lattice disorder, while elastic collisions involve significant displacement of lattice atoms and thus cause significant local crystal damage. The relative contribution of these two collision mechanisms to ion energy loss varies with incident-ion energy. Electronic excitations predominate at high energy, whereas nuclear damage dominates for low energy. As a result, high-energy

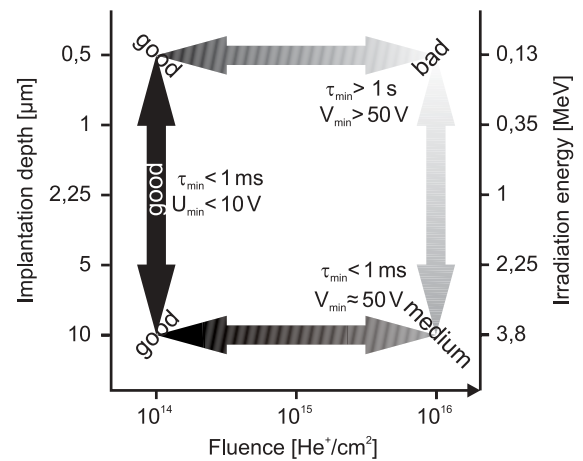


Figure 5. Schematic illustration of poling quality dependence on the He implantation parameters.

ions first lose their energy through electronic excitations in the near-surface region generating negligible damage until they reach a characteristic lower energy, at which point coupling to the lattice degrees of freedom via elastic collisions dominates. During the elastic-collision phase the ion energy loss is sufficiently high that damage occurs in a very narrow implantation layer. For example, the width of this highly damaged implantation layer for the irradiation with He⁺ ions in LiNbO₃ at energies of 130 keV and 3.5 MeV is 200 and 470 nm, respectively [38].

4.2. Poling behavior

The results of the poling maps obtained for samples subjected to various levels of irradiation fluence and energy (section 3.1) are summarized qualitatively in a two-dimensional plot displayed in figure 5. In general, low fluence ($\leq 10^{15}$ cm⁻²) allows for easy poling regardless of the energy used. At higher fluence, poling is hindered. The latter property is clearly seen for the case of low irradiation energy when the implanted layer is close to the surface. The qualitative notations ‘good’, ‘medium’, and ‘bad’ in figure 5 reflect both the ease of poling and the domain’s shape. ‘Good’ means the domains are circular (or hexagonal if larger than 400 nm) and can be generated readily with very modest voltage pulses (10 V; 1 ms); domain formation is successful within the whole poling map. ‘Medium’ describes poling properties that also result in well formed domains, however, their formation requires voltage pulses with higher amplitude; domain formation is successful only within 2/3 of the poling map. ‘Bad’ applies to poling, which is not only characterized by pulses of larger amplitude and longer duration but also results in a non-regular domain shape; domain formation is successful within less than 1/3 of the poling map. The knowledge of irradiation damage physics in solids (section 4.1) allows us to explain some of our observations on poling and in particular its dependence on ion fluence and energy.

First, at high fluence, the implanted layer is heavily damaged, the piezoelectricity, as observed in the investigations of cross-sections of the samples in section 3.2 and thus

presumably also the ferroelectricity, is strongly degraded. Further, at low irradiation energy, when the implanted layer is situated close to the sample surface, domain formation is hindered. On the other hand, if the irradiation energy is high, the distorted implantation layer is far below the surface, and domain formation is again possible.

Second, at low fluence, easy poling is observed, i.e. only modest voltage pulses (10 V; 1 ms) are required for domain formation, irrespective of the irradiation energy used. In this case, the implanted layer was not observed to exhibit degradation in its piezoelectricity (section 3.2). We therefore assume that the crystal is still ferroelectric within the whole He-irradiated area. As a consequence, poling is readily done at low irradiation energies, although the implanted layer is situated close to the sample surface. Consider now which physical effect, i.e. the nuclear or the electronic damage, allows for stable nanodomain formation in the samples subjected to high irradiation energy (up to $t = 10 \mu\text{m}$). To answer this question, the effect of the SPM-tip-assisted poling process is examined. Since the electric field from the SPM tip is negligible at depths below $\approx 2 \mu\text{m}$ of the sample surface, the implanted layer cannot play a crucial role in the formation of stable domains. This suggests that the electronic damage, which takes place along the entire path of the He ions inside the crystal, has a domain-stabilizing effect.

Note that (i) the domains written were observed to be stable for months under ambient conditions. Moderate heating ($T = 250^\circ\text{C}$), however, erased the domain pattern, and (ii) the poling behavior for both materials investigated, undoped and Mg-doped LiNbO_3 , was identical. Obviously the effect of electronic damage exceeds any effect from the differences between these two materials, that is a very different coercive field.

4.3. Proximity effect

The proximity effect was defined as the influence of previously written domains on the size and shape of domains written subsequently; this effect is seen, for example, in the large-area domain patterns in figures 3(b) and (c). In general, the proximity effect is observed to become more prominent as inter-domain distance is reduced. However, domains seem to interact even if their distance is much larger than their diameter. Because of this long-range interaction it is assumed that the proximity effect is of electrostatic nature; this point is further seen in the following line of reasoning. Poling of a domain implies the inversion of the surface polarization charge. Since in our experiment only surface domains are generated, residual charge from the poling accumulates at the buried end of the domain, which lies in the implantation layer. In addition, our method of domain inversion by applying voltage pulses to an SPM tip leads to charge injection into the sample surface as in a corona discharge [39]. Both of these mechanisms lead to buried charges of the same polarity in the implantation layer. For instance, poling with a positive voltage results in a positively charged end of the domain inside the crystal and leads also to the injection of holes into the sample surface. Formation of a new domain in the vicinity of previously written domains is therefore hampered by electrostatic repulsion.

Our assumption that electrostatic repulsion causes the proximity effect is further supported by the observation that the size of isolated domains increases linearly with the pulse amplitude V , but is independent of its duration τ (section 3.1). The latter is in contrast to SPM poling experiments performed on thin-film, single-crystal samples [40]. Domain growth in He-irradiated crystals is obviously restricted by the buried charges in the implantation layer as described above. The attempt to increase the conductivity of the crystal, thereby allowing for a charge flow as it takes place in the thin-film experiments via the back electrode, was done by using Mg-doped LiNbO_3 crystals and UV illumination during poling (section 3.1). This attempt was not successful since the conductivity was still not sufficiently high; this result might have been anticipated based on the results obtained with the cross-sectioned samples (section 3.2).

From a practical point of view, the proximity effect has very useful implications. These are as follows: first, domains within a large-area pattern are of the same size (excluding the domains situated at the frame). This is advantageous for any application utilizing large-area nanodomain patterns, as is required for instance for photonic crystals. The size of the individual domains (for a given inter-domain distance) can be controlled by the voltage applied to the SPM tip. Second, the domain size can be reliably scaled down to $< 100 \text{ nm}$ diameter by using voltage pulses with small amplitude together with ultra-sharp tips. There is, to date, no other method for domain formation which allows for such small domains to be written in single-crystal samples, as it is needed for most photonic applications. Third, neighboring domains do not merge. Indeed this allegedly trivial fact is of major importance, since in other domain formation techniques, lateral domain growth limits the minimum domain size and inter-domain spacing to a few micron range.

4.4. Domain shape

The shape of the domains, investigated by the multi-step procedure described in section 2.3, is shown in figure 4. For the sample that is implanted at low energy (350 keV corresponding to $t = 1 \mu\text{m}$), the etched domain is quasi-cylindrical. For the etched domains in samples implanted at higher energy (1 MeV corresponding to $t = 2.28 \mu\text{m}$) the domains are conical (figures 4(d) and (e)). This can be understood in light of the proximity effect as a consequence of electrostatic repulsion (section 4.3), which not only affects the size of the domains at the sample surface, as seen by PFM measurements (figures 3(b) and (c)), but also the evolution of the domains into the crystal.

Finally a comment is needed on the challenges that need to be taken into account when transferring a large-area nanodomain pattern into a topographical structure. The issue of lateral etching, attacking the y -faces of the crystal from inside the holes, leads automatically to a cone shape, even though etching starts with a cylindrical domain shape, as discussed above. A further issue lies in the aspect ratio of the formed nanodomains. As seen in figure 4(d) the width of the domain at the sample surface is only 500 nm, however, it reaches a depth of $\approx 2 \mu\text{m}$. Consequently, efficient HF etching

of the holes down to the bottom is hampered by the slow acid exchange at the bottom of the hole. A solution for this difficulty might be by irradiating the crystals from their $-z$ -face, thus forming $+z$ -faced surface domains, which, as a result would emerge as pillars from the etching process.

5. Conclusions

We have investigated the effect of prior He implantation of a ferroelectric crystal on the properties of domains written by local poling with an SPM tip. The effect of implantation fluence and energy on the domain formation was studied by PFM imaging and selective etching. Low-fluence implantation was found to result in better conditions for domain writing as it generates less damage. Investigation of cross-section samples has shown that the domains grow from the surface down into the implantation layer. The facile nature of domain formation at high energies implies that electrostatic damage has a stabilizing effect. In addition, the proximity effect, i.e. domain size and depth limitation by other neighboring domains, can be explained by electrostatic repulsion of poling-induced buried charges. As a result, ion implantation followed by SPM-assisted poling was found to result in a uniform domain-array formation, making it a promising method for writing of large-area nanodomain patterns.

Acknowledgments

Partial support for this work (RO, AO, OG, SB, HB) was received from the US NSF (DMR-08-0668206). Additional financial support was also received from Deutsche Telekom AG (ML, ÁH, ES). We thank Nicolae Panoiu (University College, London) for helpful discussions regarding the importance of domain feature shape for applications in photonic crystals.

References

- [1] Weis R S and Gaylord T K 1985 *Appl. Phys. A* **37** 191–203
- [2] Volk T and Wöhlecke M 2008 *Lithium Niobate: Defects, Photorefraction, and Ferroelectric Switching* (Berlin: Springer)
- [3] Buse K, Adibi A and Psaltis D 1998 *Nature* **393** 665–8
- [4] Arizmendi L 2004 *Phys. Status Solidi a* **201** 253–83
- [5] Myers L E, Eckardt R C, Fejer M M, Byer R L, Bosenberg W R and Pierce J W 1995 *J. Opt. Soc. Am. B* **12** 2102–16
- [6] Khurgin J B 2005 *Phys. Rev. A* **72** 023810
- [7] Canalias C and Pasiskevicius V 2007 *Nat. Photon.* **1** 459
- [8] Joannopoulos J D, Johnson S G and Winn J N 2008 *Photonic Crystals: Molding the Flow of Light* (Princeton, NJ: Princeton University Press)
- [9] Sohler W et al 2008 *Opt. Photon. News* **19** 24–31
- [10] Broderick N G R, Ross G W, Offerhaus H L, Richardson D J and Hanna D C 2000 *Phys. Rev. Lett.* **84** 4345–8
- [11] Schrepel F, Gischkat Th, Hartung H, Kley E-B and Wesch W 2006 *Nucl. Instrum. B* **250** 164–8
- [12] Burr G W, Diziain S and Bernal M-P 2008 *Opt. Express* **16** 6302–16
- [13] Roussey M, Bernal M-P, Courjal N, Van Labeke D, Baida F I and Salut R 2006 *Appl. Phys. Lett.* **89** 241110
- [14] Ródenas A, Lamela J, Jaque D, Lifante G, Jaque F, García-Martín A, Zhou G and Gu M 2009 *Appl. Phys. Lett.* **95** 181103
- [15] Hu H, Milenin A P, Wehrspohn R B, Hermann H and Sohler W 2006 *J. Vac. Sci. Technol. A* **24** 1012–5
- [16] Barry I E, Ross G W, Smith P G R, Eason R W and Cook G 1998 *Mater. Lett.* **37** 246–54
- [17] Sones C L, Ganguly P, Ying C Y J, Soergel E, Eason R W and Mailis S 2010 *Appl. Phys. Lett.* **97** 151112
- [18] Ying C Y J, Sones C L, Peacock A C, Johann F, Soergel E, Eason R W, Zervas M N and Mailis S 2010 *Opt. Express* **18** 11508–13
- [19] Sones C L, Muir A C, Ying Y J, Mailis S, Eason R W, Jungk T, Hoffmann Á and Soergel E 2008 *Appl. Phys. Lett.* **92** 072905
- [20] Steigerwald H, Luedtke F and Buse K 2009 *Appl. Phys. Lett.* **94** 032906
- [21] Ishizuki H, Shoji I and Taira T 2003 *Appl. Phys. Lett.* **82** 4062–4
- [22] Lilienblum M, Ofan A, Hoffmann Á, Gaathon O, Vanamurthy L, Bakhru S, Bakhru H, Osgood R M Jr and Soergel E 2010 *Appl. Phys. Lett.* **96** 082902
- [23] Radojevic A M, Levy M, Osgood R M Jr, Kumar A, Bakhru H, Tian C and Evans C 1999 *Appl. Phys. Lett.* **74** 3197–9
- [24] Bryan D A, Gerson R and Tomaschke H E 1984 *Appl. Phys. Lett.* **44** 847
- [25] Maruyama M, Nakajima H, Kurimura S, Yu N E and Kitamura K 2006 *Appl. Phys. Lett.* **89** 011101
- [26] Wengler M C, Fassbender B, Soergel E and Buse K 2004 *J. Appl. Phys.* **96** 2816–20
- [27] Wengler M C, Heinemeyer U, Soergel E and Buse K 2005 *J. Appl. Phys.* **98** 064104
- [28] Jungk T, Hoffmann Á and Soergel E 2008 *New J. Phys.* **10** 013019
- [29] Johann F, Ying Y J, Jungk T, Hoffmann Á, Sones C L, Eason R W, Mailis S and Soergel E 2009 *Appl. Phys. Lett.* **94** 172904
- [30] Alexe M and Gruverman A (ed) 2004 *Nanoscale Characterisation of Ferroelectric Materials* (Berlin: Springer)
- [31] Stern J E, Terris B D, Mamin H J and Rugar D 1988 *Appl. Phys. Lett.* **53** 2717–9
- [32] Johann F, Hoffmann Á and Soergel E 2010 *Phys. Rev. B* **81** 094109
- [33] Johann F and Soergel E 2009 *Appl. Phys. Lett.* **95** 232906
- [34] Jungk T, Hoffmann Á and Soergel E 2009 *New J. Phys.* **11** 033029
- [35] Sones C L, Mailis S, Brocklesby W S, Eason R W and Owen J R 2002 *J. Mater. Chem.* **12** 295–8
- [36] Sones C L 2008 private communication
- [37] Ziegler J F 1984 *Ion Implantation Science and Technology* (Orlando: Academic)
- [38] Ziegler J 2006 SRIM <http://www.srim.org>
- [39] Bühlmann S, Colla E and Muralt P 2005 *Phys. Rev. B* **72** 214120
- [40] Kingon A, Gruverman A, Kalinin S V, Terabe K, Liu X Y, Rodriguez B J, Nemanich R J and Kitamura K 2005 *Appl. Phys. Lett.* **86** 012906